

Article

Implicit finite element implementation of Chaboche's plasticity kinematic hardening model

Cardoso, R.A. ^{1,*}

¹ Department of Mechanical Engineering, Federal University of Rio Grande do Norte 59078-970 Natal, RN, Brazil;
raphael.araujo@ufrn.br

Received: 08/06/2021; Accepted: 15/07/2021; Published: 17/09/2021

Abstract: In the context of cyclic plasticity, Chaboche's kinematic hardening model is well-known once it is capable of properly capturing the Bauschinger effect. In spite of its relative simplicity, Chaboche's model allows a good description of material nonlinearities for ductile metallic materials. In this setting, this paper aims to present a comprehensive guideline for the implementation of Chaboche's plasticity kinematic hardening model in the context of finite element analysis. A detailed strategy for the resolution of the elastoplastic problem (return mapping) as well as for the computation of the consistent tangent operator are presented. Both 2D and 3D numerical implementation strategies are addressed. In the end, a few numerical examples are presented demonstrating the accuracy and applicability of the methodology presented, where analytical solutions were used for validation. This paper also investigates the influence of the implicit integration strategy employed in the resolution of the elastoplastic equations showing that, for the material and loading conditions here assessed, results from a fully implicit integration scheme are nearly identical to those obtained by a standard trapezoidal rule.

Keywords: Plasticity; Kinematic Hardening; Finite Element Analysis

1. Introduction

Lately, strong optimum designing requirements such as weight reduction and structural reliability made by the modern industry forces constantly researches and engineers to use more sophisticated material models. In the context of ductile metals subjected to cyclic loads, the use of kinematic hardening rules properly accounting material's elastoplastic behaviour might become strongly necessary mainly in the low cycle fatigue regime, where plastic strains may inevitably occur. In this setting, Chaboche's kinematic hardening model (Chaboche, 1986) standouts once it is capable of properly capturing the Bauschinger effect, which is exhibited, with more or less extent, by ductile metals experiencing cyclic loads. This paper presents a detailed procedure for the implementation of the well-known Chaboche's model in the context of finite element (FE) analysis when considering small strains. For so, von Mises yield surface and an associative flow rule are adopted in the resolution of the elastoplastic problem. Besides, rather than focusing on the applicability and limitations of the nonlinear kinematic rule considered in this work, attention is paid to the formulation and development of all the equations necessary for implementation in FE applications. In the next, one presents the fundamental mathematical relations governing the problem studied.

According to von Mises yield criterion we have the following yield function:

$$f = \|\mathbf{S}\| - \sqrt{2/3} \bar{\sigma}_y \leq 0 \quad (1)$$

where a given material is under the elastic regime whenever $f < 0$, \mathbf{S} is the deviatoric part of Cauchy's stress tensor, $\boldsymbol{\sigma}$, and $\bar{\sigma}_y$ is the material initial yield stress. On the other hand, $f = 0$ in Eq. (1) implies that the material is experiencing plastic flow. When considering kinematic hardening behavior (Prager, 1949; Armstrong and Frederick,

1966; Chaboche, 1986), Eq. (1) can be modified by assuming that the elastic domain can be shifted on the deviatoric stress space while keeping its shape unchanged (translation):

$$f = \|\mathbf{S} - \boldsymbol{\beta}\| - \sqrt{2/3} \bar{\sigma}_y \leq 0 \quad (2)$$

where $\boldsymbol{\beta}$ is the back stress tensor. According to Chaboche's model (Chaboche, 1986), for time-independent plastic behaviour, the back stress tensor can be decomposed in a number (m) of Armstrong and Frederick nonlinear kinematic hardening rules:

$$\dot{\boldsymbol{\beta}} = \sum_{i=1}^m \dot{\boldsymbol{\beta}}_i \quad (3)$$

$$\dot{\boldsymbol{\beta}}_i = \frac{2}{3} H_i \dot{\boldsymbol{\epsilon}}^p - \sqrt{\frac{2}{3}} b_i \boldsymbol{\beta}_i \|\dot{\boldsymbol{\epsilon}}^p\| \quad (4)$$

where H_i and b_i are material parameters, which can be obtained from tension-compression tests and $\dot{\boldsymbol{\epsilon}}^p$ is the plastic strain rate. The latter can be defined as:

$$\dot{\boldsymbol{\epsilon}}^p = \dot{\gamma} \mathbf{N} \quad (5)$$

where $\dot{\gamma}$ is the plastic multiplier rate and \mathbf{N} , by assuming an associative hardening rule, can be expressed as:

$$\mathbf{N} = \frac{\partial f}{\partial \boldsymbol{\sigma}} \quad (6)$$

By differentiating Eq. (2) with respect to $\boldsymbol{\sigma}$:

$$\mathbf{N} = \frac{\mathbf{S} - \boldsymbol{\beta}}{\|\mathbf{S} - \boldsymbol{\beta}\|} \quad (7)$$

Notice that, the plastic multiplier rate, $\dot{\gamma}$, and the yield surface, f , must obey the following relation:

$$\dot{\gamma} f = 0 \quad (8)$$

Eq. (8) is commonly referred as Kuhn-Tucker complementary conditions, where, if the material experiences plastic flow, $\dot{\gamma} > 0$ and $f = 0$, otherwise, under purely elastic strain rates, $\dot{\gamma} = 0$ and $f < 0$.

Elastoplasticity models like the one here presented are mostly integrated by means of the radial return algorithm (Wilkins, 1963; Simo and Taylor, 1986; Malcher and Mamiya, 2014; Lopes and Malcher, 2017). In this type of algorithm, a purely elastic trial state is commonly followed by a plastic corrector phase (return mapping procedure). In the next section, a generic implicit integration scheme for the resolution of the elastoplastic problem is presented, where it starts by assuming that the total plastic strain rate, $\dot{\boldsymbol{\epsilon}}$, can be additively decomposed as:

$$\dot{\boldsymbol{\epsilon}} = \dot{\boldsymbol{\epsilon}}^e + \dot{\boldsymbol{\epsilon}}^p \quad (9)$$

It is worth mentioning that there are many numerical strategies available in the literature for the numerical integration and resolution of cyclic plasticity models such as the one addressed in this work. Most of them make use of implicit methods for the integration of time rate variables. Even though explicit methods are easier to implement, they demand fine loading history discretizations in order to provide accurate solutions, which might become prohibitive when considering the computational cost in FE analyses. Concerning the implicit methods, this work presents a more generic approach, which can be easily reproduced in the implementation of more complex cyclic plasticity models. However, it should be pointed out that there are other strategies in the literature based on the reduction, through mathematical manipulations, of the unknown variables appearing in the resolution of elastoplastic problem (Hartmann and Haupt, 1993; Hopperstad and Remseth, 1995; Ohno *et al.*, 2013). In (Doghri, 1993), on the other hand, authors focus on the determination of closed form expressions that can be explicitly evaluated in the application of the Newton-Raphson method during problem's resolution. Once this approach avoids the successive resolution of linear systems, it is computationally more efficient. However, its application depends on the obtaining of closed form equations that might be unlikely for complex plasticity models.

The remaining of the paper is organized as follows: Section 2 details the strategy concerning the integration and resolution of the elastoplastic problem. It also presents the procedure used to obtain the consistent tangent matrix, which is necessary in the FE computations. The FE formulation on the other hand is addressed in Section 3. In Section 4, numerical examples are solved allowing the validation of the numerical procedures detailed in this work. Finally, Section 5 addresses conclusions and final remarks.

2. Integration elastoplastic problem

2.1 Basic formulation

Let $[0, T] \subset \mathbb{R}$ be the time of interest in the resolution of a given problem. Assume that the solution of the problem is known up to $t_n \in [0, T]$, which includes elastic and plastic variables. In this case, for $t_{n+1} \in [0, T]$, the trial elastic strain tensor is defined as:

$$\boldsymbol{\varepsilon}^{e\,trial} = \boldsymbol{\varepsilon}_n^e + \Delta\boldsymbol{\varepsilon} \quad (10)$$

where $\Delta\boldsymbol{\varepsilon}$ comes from the resolution of the FE problem at t_{n+1} . Note that the trial state is nothing but assuming that the strain increment $\Delta\boldsymbol{\varepsilon}$ is purely elastic (Eq. (9)).

From Eq. (10) the trial stress at t_{n+1} can be readily obtained through Hooke's law:

$$\boldsymbol{\sigma}^{trial} = \mathbb{D} : \boldsymbol{\varepsilon}^{e\,trial} \quad (11)$$

where \mathbb{D} is Hooke's linear elastic tensor.

Once the trial state assumes that $\Delta\boldsymbol{\varepsilon}$ is purely elastic, we conclude that the trial plastic variables remain unchanged in $[t_n, t_{n+1}]$, i.e.

$$\boldsymbol{\varepsilon}^{p\,trial} = \boldsymbol{\varepsilon}_n^p \quad (12)$$

and

$$\boldsymbol{\beta}^{trial} = \boldsymbol{\beta}_n \quad (13)$$

From Eqs. (11) and (13) we can compute the trial yield function:

$$f^{trial} = \|\mathbf{S}^{trial} - \boldsymbol{\beta}^{trial}\| - \sqrt{\frac{2}{3}}\bar{\sigma}_y \quad (14)$$

where if $f^{trial} < 0$, the trial state holds true and all the variables at t_{n+1} can be updated according to:

$$(*)_{n+1} = (**)_{n+1}^{trial} \quad (15)$$

Otherwise, the process is elastoplastic in $[t_n, t_{n+1}]$ and the return mapping (plastic corrector) procedure described below has to be applied, which consists in satisfying the following set of nonlinear equations:

$$\boldsymbol{\sigma}_{n+1} = \boldsymbol{\sigma}^{trial} - \Delta\gamma\mathbb{D} : [\alpha\mathbf{N}_{n+1} + (1 - \alpha)\mathbf{N}_n] \quad (16)$$

$$\boldsymbol{\beta}_{i,n+1} = \boldsymbol{\beta}_{i,n} + \frac{2}{3}H_i\Delta\gamma[\alpha\mathbf{N}_{n+1} + (1 - \alpha)\mathbf{N}_n] - \sqrt{\frac{2}{3}}b_i[\alpha\boldsymbol{\beta}_{i,n+1} + (1 - \alpha)\boldsymbol{\beta}_{i,n}]\Delta\gamma \quad (17)$$

$$\|\mathbf{S}_{n+1} - \boldsymbol{\beta}_{n+1}\| - \sqrt{\frac{2}{3}}\bar{\sigma}_y = 0 \quad (18)$$

where the unknowns are $\boldsymbol{\sigma}_{n+1}$, $\boldsymbol{\beta}_{i,n+1}$ ($i = 1$ to m) and $\Delta\gamma$. In order to obtain Eqs. (16) and (17), (i) a generalized trapezoidal integration rule has been considered, where $\alpha \in [0, 1]$, (ii) $\Delta\boldsymbol{\varepsilon}^p$ has been obtained from the numerical integration of Eq. (5), i.e. $\Delta\boldsymbol{\varepsilon}^p = \Delta\gamma[\alpha\mathbf{N}_{n+1} + (1 - \alpha)\mathbf{N}_n]$ and (iii) Eq. (16) was obtained by deducting the "stress contribution" of the plastic strain increment ($\mathbb{D} : \Delta\boldsymbol{\varepsilon}^p$) in the trial stress (Eq. (11)). Finally, Eq. (18) is simply the enforcement of Eq. (8) when plastic flow takes place, i.e. $f = 0$. The procedure for the resolution of this system of equations is presented in the next subsection.

2.2 Resolution of the elastoplastic problem

The system of nonlinear equations formed by Eqs. (16)-(18) can be efficiently solved through the quadratically convergent Newton-Raphson method (Souza Neto *et al.*, 2011). In this setting, let one defines the following residuals for this system of equations:

$$\mathbf{R}_{\boldsymbol{\sigma}_{n+1}} = \boldsymbol{\sigma}_{n+1} - \boldsymbol{\sigma}^{trial} + \Delta\gamma\mathbb{D} : [\alpha\mathbf{N}_{n+1} + (1 - \alpha)\mathbf{N}_n] \quad (19)$$

$$\mathbf{R}_{\boldsymbol{\beta}_{i,n+1}} = \boldsymbol{\beta}_{i,n+1} - \boldsymbol{\beta}_{i,n} - \frac{2}{3}H_i\Delta\gamma\mathbf{Q}^{-1}[\alpha\mathbf{N}_{n+1} + (1 - \alpha)\mathbf{N}_n] + \sqrt{\frac{2}{3}}b_i[\alpha\boldsymbol{\beta}_{i,n+1} + (1 - \alpha)\boldsymbol{\beta}_{i,n}]\Delta\gamma \quad (20)$$

$$R_{f_{n+1}} = \sqrt{(\mathbf{S}_{n+1} - \boldsymbol{\beta}_{n+1})^T \mathbf{Q} (\mathbf{S}_{n+1} - \boldsymbol{\beta}_{n+1})} - \sqrt{\frac{2}{3}}\bar{\sigma}_y \quad (21)$$

where, for the sake of convenience, terms appearing in Eqs. (16)-(18) were rewritten in matrix form according to the following definitions:

$$\boldsymbol{\sigma} = [\sigma_x \quad \sigma_y \quad \sigma_z \quad \tau_{xy} \quad \tau_{xz} \quad \tau_{yz}]^T \quad (22)$$

$$\boldsymbol{\beta} = [\beta_x \quad \beta_y \quad \beta_z \quad \beta_{xy} \quad \beta_{xz} \quad \beta_{yz}]^T \quad (23)$$

$$\boldsymbol{\varepsilon} = [\varepsilon_x \quad \varepsilon_y \quad \varepsilon_z \quad 2\varepsilon_{xy} \quad 2\varepsilon_{xz} \quad 2\varepsilon_{yz}]^T \quad (24)$$

$$\boldsymbol{\varepsilon}^p = [\varepsilon_x^p \quad \varepsilon_y^p \quad \varepsilon_z^p \quad 2\varepsilon_{xy}^p \quad 2\varepsilon_{xz}^p \quad 2\varepsilon_{yz}^p]^T \quad (25)$$

$$\mathbf{S} = \mathbf{P}\boldsymbol{\sigma} \quad (26)$$

$$f = \sqrt{(\mathbf{S} - \boldsymbol{\beta})^T \mathbf{Q} (\mathbf{S} - \boldsymbol{\beta})} - \sqrt{\frac{2}{3}} \bar{\sigma}_y \quad (27)$$

Expressions for the Hooke's matrix, \mathbf{D} , the deviatoric transformation, \mathbf{P} , and the matrix \mathbf{Q} are given in Appendix A. The matrix, \mathbf{Q} , apropos, is a linear transformation which yields $(\mathbf{S} - \boldsymbol{\beta})^T \mathbf{Q} (\mathbf{S} - \boldsymbol{\beta}) = (\mathbf{S} - \boldsymbol{\beta}) : (\mathbf{S} - \boldsymbol{\beta})$. Notice that, \mathbf{N} , Eqs. (19) and (20), is defined as follows:

$$\mathbf{N} = \frac{\mathbf{Q}(\mathbf{S} - \boldsymbol{\beta})}{\sqrt{(\mathbf{S} - \boldsymbol{\beta})^T \mathbf{Q} (\mathbf{S} - \boldsymbol{\beta})}} \quad (28)$$

In this case, it is also worth noting that \mathbf{Q}^{-1} appearing in Eq. (20) is introduced in order to ensure consistency with the definition of the back stress terms (see Eqs. (4), (5) and (7)).

With the residual equations in hands, the Newton-Raphson scheme leads to the solution of the following linearized system:

$$\begin{bmatrix} \frac{\partial \mathbf{R}_{\sigma_{n+1}}}{\partial \sigma_{n+1}} & \frac{\partial \mathbf{R}_{\sigma_{n+1}}}{\partial \beta_{j,n+1}} & \frac{\partial \mathbf{R}_{\sigma_{n+1}}}{\partial \Delta\gamma} \\ \frac{\partial \mathbf{R}_{\beta_{i,n+1}}}{\partial \sigma_{n+1}} & \frac{\partial \mathbf{R}_{\beta_{i,n+1}}}{\partial \beta_{j,n+1}} & \frac{\partial \mathbf{R}_{\beta_{i,n+1}}}{\partial \Delta\gamma} \\ \frac{\partial R_{f_{n+1}}}{\partial \sigma_{n+1}} & \frac{\partial R_{f_{n+1}}}{\partial \beta_{j,n+1}} & \frac{\partial R_{f_{n+1}}}{\partial \Delta\gamma} \end{bmatrix}^{(k)} \begin{bmatrix} \delta \sigma_{n+1} \\ \delta \beta_{j,n+1} \\ \delta \Delta\gamma \end{bmatrix} = - \begin{bmatrix} \mathbf{R}_{\sigma_{n+1}} \\ \mathbf{R}_{\beta_{i,n+1}} \\ R_{f_{n+1}} \end{bmatrix}^{(k)} \quad (29)$$

where at the end of k^{th} iteration, the problem's solution is given by:

$$\boldsymbol{\sigma}_{n+1}^{k+1} = \boldsymbol{\sigma}_{n+1}^k + \delta \boldsymbol{\sigma}_{n+1} \quad (30)$$

$$\boldsymbol{\beta}_{j,n+1}^{k+1} = \boldsymbol{\beta}_{j,n+1}^k + \delta \boldsymbol{\beta}_{j,n+1} \quad (31)$$

$$\Delta\gamma^{k+1} = \Delta\gamma^k + \delta \Delta\gamma \quad (32)$$

This iterative process is terminated when convergence is achieved. The derivatives appearing in Eq. (29) are given in Appendix A. δ in Eqs. (29)-(32) denotes increments of the unknown variables towards the problem's solution.

2.3. Consistent tangent matrix computation

This section presents the derivation of the consistent tangent matrix. In order to ensure a quadratic rate of convergence of the Newton-Raphson method in the FE analysis, the consistent tangent matrix needs to be computed as follows (more details in Section 3):

$$\mathbf{D}^{ep} = \frac{\partial \boldsymbol{\sigma}_{n+1}}{\partial \boldsymbol{\varepsilon}_{n+1}} \quad (33)$$

In this case, recall that from the resolution of the elastoplastic problem provided in the last subsection, the following set of equations holds true:

$$\boldsymbol{\varepsilon}_{n+1} - \boldsymbol{\varepsilon}^{e^{trial}} + \Delta\gamma[\alpha \mathbf{N}_{n+1} + (1 - \alpha) \mathbf{N}_n] = \mathbf{0} \quad (34)$$

$$\boldsymbol{\beta}_{i,n+1} - \boldsymbol{\beta}_{i,n} - \frac{2}{3} H_i \Delta\gamma \mathbf{Q}^{-1} [\alpha \mathbf{N}_{n+1} + (1 - \alpha) \mathbf{N}_n] + \sqrt{\frac{2}{3}} b_i [\alpha \boldsymbol{\beta}_{i,n+1} + (1 - \alpha) \boldsymbol{\beta}_{i,n}] \Delta\gamma = \mathbf{0} \quad (35)$$

$$\sqrt{(\mathbf{S}_{n+1} - \boldsymbol{\beta}_{n+1})^T \mathbf{Q} (\mathbf{S}_{n+1} - \boldsymbol{\beta}_{n+1})} - \sqrt{\frac{2}{3}} \bar{\sigma}_y = 0 \quad (36)$$

The linearization of the above system of equations leads to:

$$\begin{bmatrix} \mathbf{M}_{11} & \mathbf{M}_{12} & \mathbf{M}_{13} \\ \mathbf{M}_{21} & \mathbf{M}_{22} & \mathbf{M}_{23} \\ \mathbf{M}_{31} & \mathbf{M}_{32} & 0 \end{bmatrix} \begin{bmatrix} d\boldsymbol{\sigma} \\ d\boldsymbol{\beta}_j \\ d\Delta\gamma \end{bmatrix} = \begin{bmatrix} d\boldsymbol{\varepsilon} \\ \mathbf{0} \\ 0 \end{bmatrix} \quad (37)$$

where

$$\mathbf{M}_{11} = \mathbf{D}^{-1} + \alpha\Delta\gamma \frac{\partial \mathbf{N}}{\partial \boldsymbol{\sigma}} \quad (38)$$

$$\mathbf{M}_{12} = \alpha\Delta\gamma \frac{\partial \mathbf{N}}{\partial \boldsymbol{\beta}_j} \quad (39)$$

$$\mathbf{M}_{13} = \tilde{\mathbf{N}} \quad (40)$$

$$\mathbf{M}_{21} = -\frac{2}{3} H_i \alpha \Delta\gamma \mathbf{Q}^{-1} \frac{\partial \mathbf{N}}{\partial \boldsymbol{\sigma}} \quad (41)$$

$$\mathbf{M}_{22} = \delta_{ij} \left(1 + \sqrt{\frac{2}{3}} b_i \alpha \Delta\gamma \right) \mathbf{I} - \frac{2}{3} H_i \alpha \Delta\gamma \mathbf{Q}^{-1} \frac{\partial \mathbf{N}}{\partial \boldsymbol{\beta}_j} \quad (42)$$

$$\mathbf{M}_{23} = -\left(\frac{2}{3} H_i \mathbf{Q}^{-1} \tilde{\mathbf{N}} - \sqrt{\frac{2}{3}} b_i \tilde{\boldsymbol{\beta}}_i \right) \quad (43)$$

$$\mathbf{M}_{31} = \mathbf{N}^T \quad (44)$$

$$\mathbf{M}_{32} = \frac{\partial f}{\partial \boldsymbol{\beta}_j}, \quad \frac{\partial f}{\partial \boldsymbol{\beta}_j} = -\mathbf{N}^T \quad (45)$$

For the sake of notation convenience, subscripts $n+1$ have been dropped as well as $\tilde{\mathbf{N}}$ and $\tilde{\boldsymbol{\beta}}_i$ were defined according to:

$$\tilde{\mathbf{N}} = \alpha \mathbf{N}_{n+1} + (1 - \alpha) \mathbf{N}_n \quad (46)$$

$$\tilde{\boldsymbol{\beta}}_i = \alpha \boldsymbol{\beta}_{i,n+1} + (1 - \alpha) \boldsymbol{\beta}_{i,n} \quad (47)$$

Expressions for $\partial \mathbf{N} / \partial \boldsymbol{\sigma}$ and $\partial \mathbf{N} / \partial \boldsymbol{\beta}_j$ are given in Appendix A and δ_{ij} in Eq. (42) refers to the Kronecker delta. It is also worth noticing that, in the linearization of Eqs. (34)-(36), the following relations have been used:

$$d\boldsymbol{\varepsilon}^e = \mathbf{D}^{-1} d\boldsymbol{\sigma}, \quad d\boldsymbol{\varepsilon}^{e,trial} = d\boldsymbol{\varepsilon} \quad (48)$$

Finally, from the inversion of Eq. (37) one has:

$$\begin{bmatrix} d\boldsymbol{\sigma} \\ d\boldsymbol{\beta}_j \\ d\Delta\gamma \end{bmatrix} = \begin{bmatrix} \mathbf{M}_{11} & \mathbf{M}_{12} & \mathbf{M}_{13} \\ \mathbf{M}_{21} & \mathbf{M}_{22} & \mathbf{M}_{23} \\ \mathbf{M}_{31} & \mathbf{M}_{32} & 0 \end{bmatrix}^{-1} \begin{bmatrix} d\boldsymbol{\varepsilon} \\ \mathbf{0} \\ 0 \end{bmatrix} \quad (49)$$

which leads to:

$$\mathbf{D}^{ep} = [\mathbf{M}^{-1}]_{11} \quad (50)$$

where $[\mathbf{M}^{-1}]_{11}$ represents the matrix that relates $d\boldsymbol{\sigma}$ with $d\boldsymbol{\varepsilon}$.

2.4 Particularizing for 2D analyses

In the previous subsection, all formulations concerning the resolution of the elastoplastic problem were set considering generic 3D problems. For the resolution of 2D problems, a few modifications have to be made.

When dealing with plane strain or axisymmetric problems, these modifications are straightforward. In this case, in the definition of $\boldsymbol{\sigma}$, $\boldsymbol{\beta}_i$, $\boldsymbol{\varepsilon}$ and $\boldsymbol{\varepsilon}^p$, Eqs. (22)-(25), we only need to remove the last two terms of these matrices, i.e. the

$(*)_{xz}$ and $(*)_{yz}$ components. Consequently, the matrices \mathbf{P} , Eq. (26), and \mathbf{Q} , Eq. (27), have their last two rows and columns removed becoming 4×4 matrices. After so, the whole resolution procedure presented in the last subsections remains the same.

More specifically, for plane strain assumptions, the $\Delta \varepsilon_z$ component of the total strain increment is always 0. In this setting, after the computation of the consistent tangent matrix, \mathbf{D}^{ep} (4×4 matrix), its 3rd row and 3rd column might be removed generating a 3×3 matrix as input for FE computations.

For plane stress constraint enforcement (i.e. $\sigma_z = 0$), a few additional changes have to be made. For more details, the reader is referred to appendix B.

3. FE formulation

Consider that Ω is the domain occupied by a given body with open boundaries that at a certain time instant $t \in [0, T] \subset \mathbb{R}$ can be distinguished in two different sets Γ_d and Γ_σ . The first one is the part of the boundary where displacements are prescribed, whereas, the second one holds for the part of the boundary where external tractions, \mathbf{f}_t , are prescribed. In this setting, for small strains and quasi-static conditions, the equilibrium equation of this problem can be expressed in terms of its weak formulation by:

$$\int_{\Omega} \boldsymbol{\varepsilon}(\mathbf{w})^T \boldsymbol{\sigma} d\Omega = \int_{\Omega} \mathbf{w}^T \mathbf{f}_b d\Omega + \int_{\Gamma_\sigma} \mathbf{w}^T \mathbf{f}_t d\Gamma, \quad \forall \mathbf{w} \in \mathcal{W} \quad (51)$$

for the following solution and weighting spaces, respectively:

$$\mathcal{U}_t = \{\mathbf{u}(t): \Omega \rightarrow \mathbb{R}^3 | \mathbf{u}(t) \in H^1(\Omega), \mathbf{u}(t) = \mathbf{u}_d \text{ in } \Gamma_d\} \quad (52)$$

$$\mathcal{W} = \{\mathbf{w}: \Omega \rightarrow \mathbb{R}^3 | \mathbf{w} \in H^1(\Omega), \mathbf{w} = \mathbf{0} \text{ in } \Gamma_d\} \quad (53)$$

where \mathbf{u} is displacement field, \mathbf{f}_b the body forces and \mathbf{w} is the weight function. For the sake of convenience, problem's weak formulation has been expressed in matrix notation. In this setting, by considering the FE method approximations (Fish, 2007; Kim, 2014), i.e. $\mathbf{w} = \mathbf{N}(\mathbf{x})\mathbf{W}$ and $\boldsymbol{\varepsilon}(\mathbf{w}) = \mathbf{B}(\mathbf{x})\mathbf{W}$, Eq. (51) becomes:

$$\mathbf{W}^T \left(\int_{\Omega} \mathbf{B}^T \boldsymbol{\sigma} d\Omega - \int_{\Omega} \mathbf{N}^T \mathbf{f}_b d\Omega - \int_{\Gamma_\sigma} \mathbf{N}^T \mathbf{f}_t d\Gamma \right) = 0 \quad (54)$$

where \mathbf{W} are the nodal values of the weight function \mathbf{w} , \mathbf{N} is the FE polynomial shape function and \mathbf{B} is the operator that relates nodal displacements with strain over the domain Ω . For the resolution of linear elastic problems, Eq. (54) can be readily solved through the resolution of a linear system. However, if considering material nonlinearities, such as the one addressed in this paper, Eq. (54) cannot be solved directly and iterative procedures like the Newton-Raphson scheme have to be applied. In this case, let us first define the following residual at the k^{th} iteration:

$$\mathbf{R}^k = \int_{\Omega} \mathbf{B}^T \boldsymbol{\sigma}^k d\Omega - \int_{\Omega} \mathbf{N}^T \mathbf{f}_b d\Omega - \int_{\Gamma_\sigma} \mathbf{N}^T \mathbf{f}_t d\Gamma \quad (55)$$

Notice that for $\mathbf{R} = \mathbf{0}$ Eqs. (54) and (55) are equivalent due to the arbitrariness of \mathbf{W} .

Therefore, the Newton-Raphson iteration scheme in the resolution of the residue \mathbf{R} leads to the solution of the following linearized problem:

$$\mathbf{K}_t^k \delta \mathbf{U} = -\mathbf{R}^k \quad (56)$$

$$\mathbf{U}^{k+1} = \mathbf{U}^k + \delta \mathbf{U} \quad (57)$$

where \mathbf{U} are the nodal displacements and the tangent stiffness matrix is given by:

$$\mathbf{K}_t = \frac{\partial \mathbf{R}}{\partial \mathbf{U}}, \quad \mathbf{K}_t = \int_{\Omega} \mathbf{B}^T \mathbf{D}^{ep} \mathbf{B} d\Omega \quad (58)$$

with \mathbf{D}^{ep} defined as:

$$\mathbf{D}^{ep} = \frac{\partial \boldsymbol{\sigma}}{\partial \boldsymbol{\varepsilon}} \quad (59)$$

For purely elastic strain increments, \mathbf{D}^{ep} , is simply given by the Hooke's matrix, \mathbf{D} , otherwise, for elastoplastic steps, it is obtained from the return mapping procedure presented in the last section.

For implementation purposes, see Boxes 1 and 2. The former summarizes the algorithmic procedures for the solution of the elastoplastic FE problem. The latter focuses on the resolution of the elastoplastic problem itself.

Box 1: Resolution FE problem	
Input: Material parameters, displacement field, elastic variables, plastic variables and FE tangent matrix at t_n and boundary conditions at t_{n+1}	
Output: Displacement field, elastic variables, plastic variables, and FE tangent matrix at t_{n+1}	
Initialization: $k = 0$, $\mathbf{U}_{n+1} = \mathbf{U}_n$, $\mathbf{K}_{t,n+1} = \mathbf{K}_{t,n}$	
$\mathbf{R}^k = \int_{\Omega} \mathbf{B}^T \boldsymbol{\sigma}_n d\Omega - \int_{\Omega} \mathbf{N}^T \mathbf{f}_{b,n+1} d\Omega - \int_{\Gamma_{\sigma}} \mathbf{N}^T \mathbf{f}_{t,n+1} d\Gamma$	
While error > tol and $k < k_{\max}$	
$\mathbf{K}_t^k \delta \mathbf{U} = -\mathbf{R}^k$ $\mathbf{U}_{n+1} \leftarrow \mathbf{U}_{n+1} + \delta \mathbf{U}$ $k \leftarrow k + 1$	
For each gauss point:	
Compute $\Delta \boldsymbol{\varepsilon} = \mathbf{B}(\mathbf{U}_{n+1} - \mathbf{U}_n)$	
Obtain \mathbf{D}^{ep} , elastic and plastic variables (Box. 2)	
End	
Update the residual \mathbf{R}_{n+1} and the tangent matrix $\mathbf{K}_{t,n+1}$, Eqs (55) and (58), respectively.	
Define a convergence criterion (for example):	
error = $\sqrt{\mathbf{R}_{n+1}^T \mathbf{R}_{n+1}}$	
End	
If $k = k_{\max}$ then convergence was not achieved.	
Reduce time step increment and repeat previous instructions.	

Box 2: Resolution elastoplastic problem	
Input: $\Delta \boldsymbol{\varepsilon}$, material parameters, elastic and plastic variables at t_n	
Output: Elastic variables, plastic variables and \mathbf{D}^{ep} at t_{n+1}	
1) Given the strain increment $\Delta \boldsymbol{\varepsilon}$ compute the trial state variables:	
$\boldsymbol{\varepsilon}^{e\,trial} = \boldsymbol{\varepsilon}_n^e + \Delta \boldsymbol{\varepsilon}, \quad \boldsymbol{\sigma}^{trial} = \mathbf{D} \boldsymbol{\varepsilon}^{e\,trial}$ $\boldsymbol{\varepsilon}^{p\,trial} = \boldsymbol{\varepsilon}_n^p, \quad \boldsymbol{\beta}^{e\,trial} = \boldsymbol{\beta}_n$	
2) Compute f^{trial} (Eq. (27) or (83)). If $f^{trial} \leq 0$ then:	
$(*)_{n+1} = (*)^{trial}$	
Otherwise, solve Eqs. (29-32) to obtain $\boldsymbol{\sigma}_{n+1}$, $\boldsymbol{\beta}_{i,n+1}$ and $\Delta \gamma$. Then calculate:	
$\Delta \boldsymbol{\varepsilon}_{n+1}^p = \Delta \gamma [\alpha \mathbf{N}_{n+1} + (1 - \alpha) \mathbf{N}_n]$	

$$\boldsymbol{\varepsilon}_{n+1}^p = \boldsymbol{\varepsilon}_n^p + \Delta \boldsymbol{\varepsilon}_{n+1}^p, \quad \boldsymbol{\varepsilon}_n^e = \boldsymbol{\varepsilon}^{e\,trial} - \Delta \boldsymbol{\varepsilon}_{n+1}^p, \quad \boldsymbol{\beta}_{n+1} = \sum \boldsymbol{\beta}_{i,n+1}$$

3) Compute the consistent tangent operator \mathbf{D}_{n+1}^{ep} (Eq. (50)). If the step is elastic, $\mathbf{D}_{n+1}^{ep} = \mathbf{D}$

4) If considering plane stress conditions:

$$\varepsilon_z^e = -\nu(\sigma_x + \sigma_y)/E, \quad \varepsilon_z^p = -(\varepsilon_x^p + \varepsilon_y^p)$$

4. Numerical examples

This paper focuses on the FE implementation of Chaboche's nonlinear kinematic hardening law. In this section, simple numerical examples are presented in order to assess the theories and implementation procedures addressed in the previous sections. Implementations were carried out in an in-house MATLAB code. In this setting, let one first consider a uniaxial tension-compression test subjected to fully reversed loading cycles. Such simple problem can be solved by considering a single plane stress element as depicted in Figure 1. Besides, this problem also possesses analytical solution, which is obtained through the exact integration of Chaboche's kinematic hardening law when considering one-dimensional plasticity (see Appendix C).

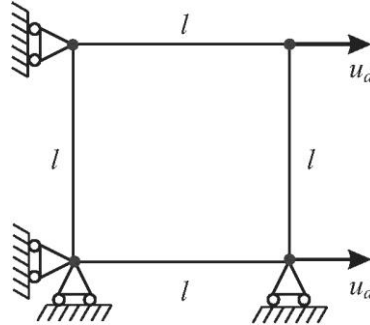


Figure 1. Uniaxial tension-compression test.

For the resolution of the FE problem, consider the plane stress element with dimension $l = 2$ mm depicted in Figure 1. The referred problem was solved considering a sinusoidal fully reversed prescribed displacement u_d varying between ± 0.4 mm (element's right edge). During the simulation, two repeated loading cycles were considered in the analysis, where each loading cycle was divided in around 25 loading increments. In addition, the following material parameters for a 7075-T651 aluminium alloy were considered in all the FE simulations presented in this paper: Young Modulus $E = 71(10^3)$ MPa, Poisson's ratio $\nu = 0.33$ and initial yield stress $\bar{\sigma}_y = 431$ MPa. The kinematic hardening terms utilized were $H_{1-3} = 8.10(10^3), 66.7(10^3), 160(10^3)$ (MPa) and $b_{1-3} = 129.8, 939.7, 0$. The determination of $\bar{\sigma}_y$, H_{1-3} and b_{1-3} followed the parameter identification procedure described in appendix D, which was applied to stabilized stress-plastic strain hysteresis loops provided in (Jiang and Zhang, 2008). Notice that here only three back stress terms were considered in the analysis ($m = 3$ in Eq. (3)) with the last one being linear, i.e. $b_3 = 0$. Generally, such assumption already reproduces properly experimental observations (Chaboche, 1986).

Figure 2 shows a comparison between the FE results and the analytic solution for the aforementioned tension-compression test. In the integration of the elastoplastic algorithm, the standard trapezoidal rule has been used, i.e. $\alpha = 1/2$ in Eqs. (16)-(17). As can be seen, a coarse loading history discretization already provides satisfactory results.

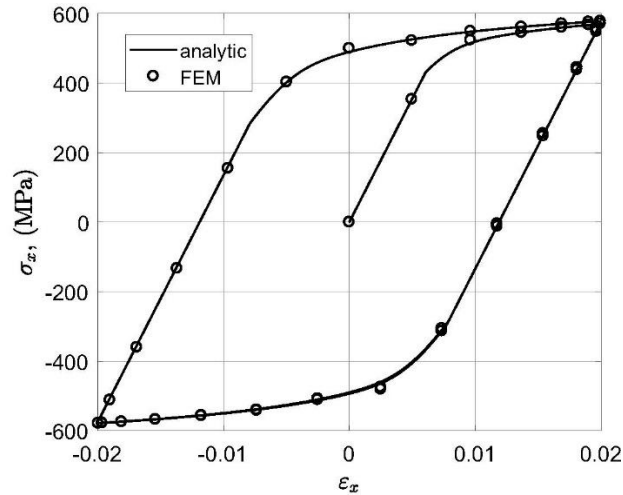


Figure 2. Uniaxial stress-strain curve.

Another very simple numerical example that can be used to validate the numerical implementations consists in modelling a pure shear cyclic test. For so, consider the schematic model depicted in Figure 3. In this case, one has a rectangular bar with length, l , and height, h . For the sake of simplicity, this problem is modelled considering plane stress enforcement. Now consider that the lower edge of such bar is clamped while its upper edge is subjected to a uniform prescribed displacement u_d in the horizontal direction. Note that the upper edge is free to move vertically. In this setting, as long as $l \gg h$ (let us say $l/h > 8$), the stress state far from the lateral edges can be regarded as pure shear (Figure 3).

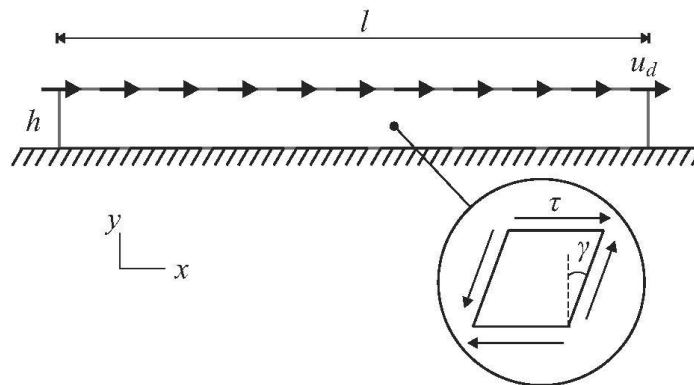


Figure 3. Schematic representation of the pure shear test.

Figure 4 compares the analytical results with the FE ones when considering $l = 10$ mm, $h = 1$ mm and a prescribed displacement, u_d , varying sinusoidally between $\pm 0,0346$ mm. As in the uniaxial test example, two loading cycles were simulated. Quadrangular linear elements with dimension 0.5 mm were used in the simulation. Each loading cycle consisted of 50 loading increments. Integration of elastoplastic equations were carried out adopting the standard trapezoidal rule. As can be seen in Figure 4, there is a good accordance between the numerical and exact solutions.

The last example here presented consists in the resolution of the axially loaded V-notched round bar problem illustrated in Figure 5. Due to the circumferential symmetry found in this problem, it was solved by considering an axisymmetric FE model. Geometry characteristics here adopted were $D = 30$ mm, $c = 3$ mm, $\rho = 0.8$ mm and $\phi = 60^\circ$. The prescribed axial stress, $\sigma(t)$, was defined according to a sinusoidal distribution with mean and amplitude values set to $\sigma_m = 120$ MPa and $\sigma_a = 160$ MPa, respectively.

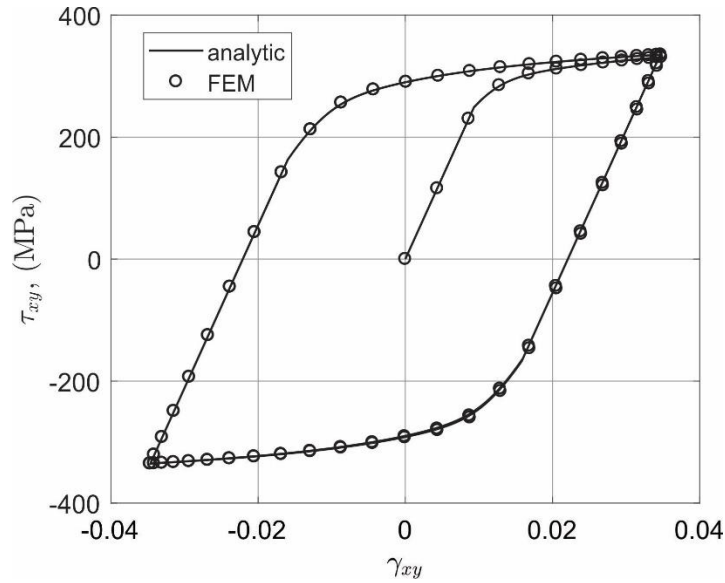


Figure 4. Shear stress-strain curve ($\gamma_{xy} = 2\varepsilon_{xy}$).

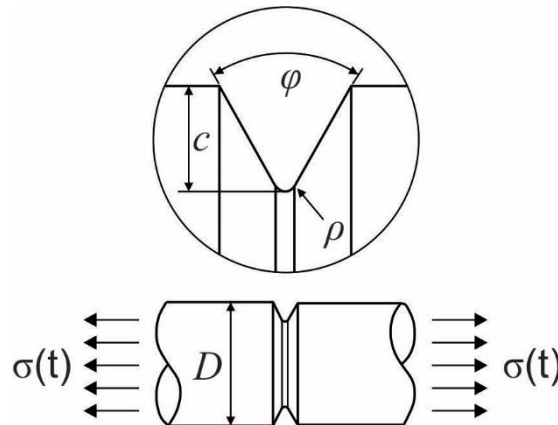


Figure 5. Schematic representation of an axially loaded V-notched round bar.

Figure 6 depicts the FE model considered in the resolution of this problem. In the simulation, loading history was split in two steps. During the first step, the mean stress σ_m is prescribed monotonically on the bar upper edge, while its left and bottom edges are prevented to displace in the horizontal and vertical directions, respectively. Notice that only one fourth of the problem is simulated due to symmetry. The second step, on the other hand, consists in prescribing the alternate stress σ_a , whereas the mean stress σ_m is held constant. Two periodic cycles are accounted in the second step. The first step was divided in 4 loading increments while each cycle of the second step was divided in 16 loading increments.

Figure 7 shows the distribution of the normal stress components along the notch bisector for the maximum prescribed stress σ (Figure 6) at second prescribed loading cycle. Differently to what happens for the elastic case, higher stresses are not observed right at the notch root. In this case, once the material experience plastic flow, residual strains at the notch root might be causing a stress relief (Liao *et al.*, 2020).

Stress-strain curves for the axial (y direction) and out of plane stress components (z) at the notch root are depicted in Figure 8. Only two loading cycles were simulated since stress-strain hysteresis remain nearly the same for further prescribed loading cycles. This figure also compares, for both these stress components, the influence of the choice of α in the integration of the elastoplastic problem. As can be seen, both values of α lead to nearly the same results. As a reminder, $\alpha = 0.5$ stands for a standard trapezoidal rule, whereas $\alpha = 1$ means a fully implicit (backward Euler) integration scheme. An $\alpha = 0$, i.e. a fully explicit (forward Euler) integration scheme, was also tested, however, it demanded load increments 4 times smaller in order to converge and lead to the same level of accuracy of the implicit integration strategies.

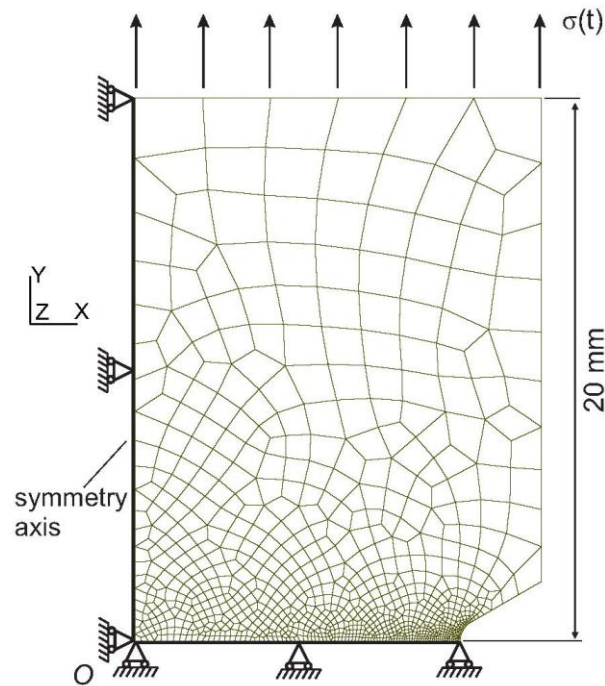


Figure 6. V-notched round bar numerical model. The coordinate system origin is at the bottom left corner (mesh generated with the free software Gmsh).

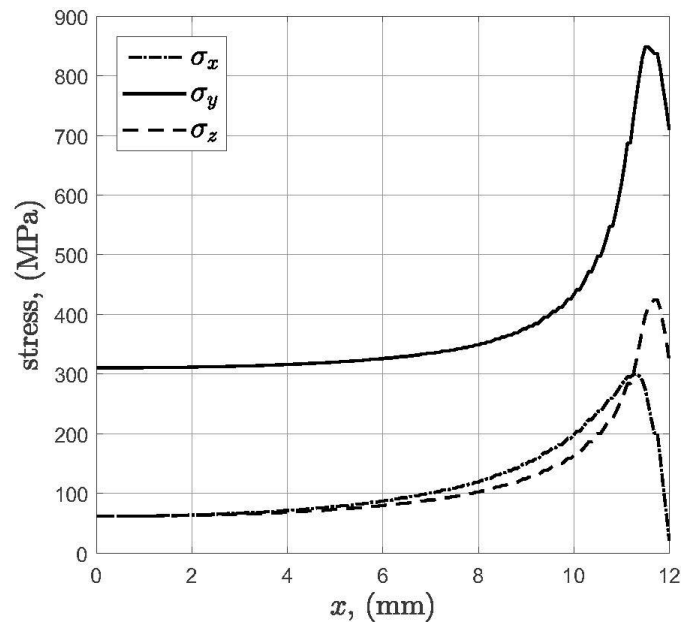


Figure 7. Maximum stress distribution along the notch bisector.

Figure 9 gives some insight concerning convergence aspects of the implicit elastoplastic FE implementation addressed in this paper. Figure 9(a) shows the convergence rate based on the Euclidean norm of the residual vector \mathbf{R}^k (Eq. (55)) for the time instants A and B illustrated in Figure 9(b). As can be seen, these results exhibit quadratic rate of convergence. It also worth highlighting that no line search procedure was necessary during the iteration process. Notice as well that time instants “A” and “B” were chosen only to illustrate the convergence behavior of the numerical method, however, same patterns are observed for other times instants.

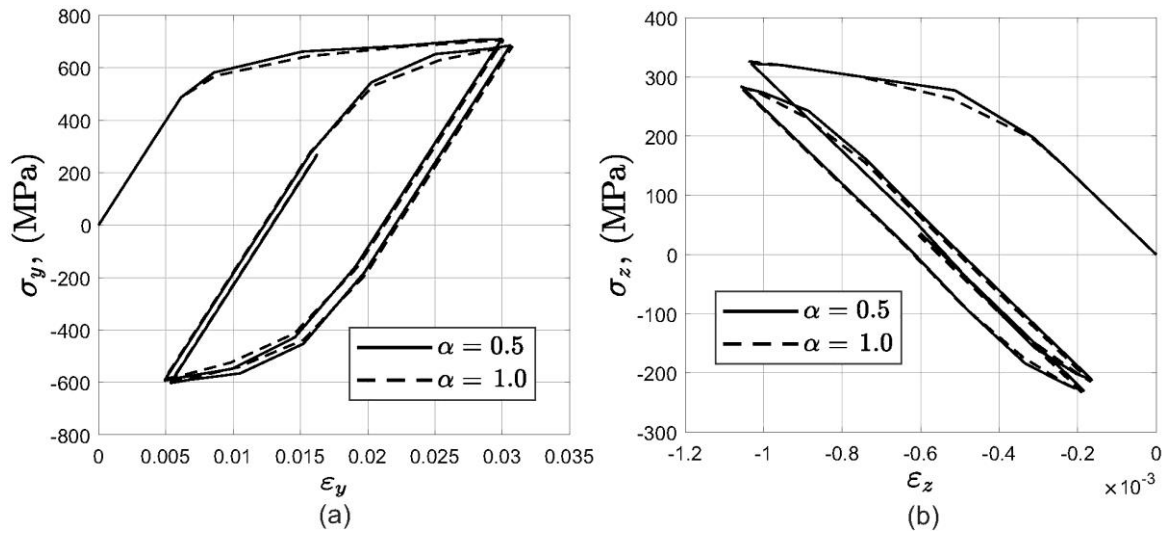


Figure 8. Stress-strain curves at the notch root: (a) axial and (b) out of plane direction.

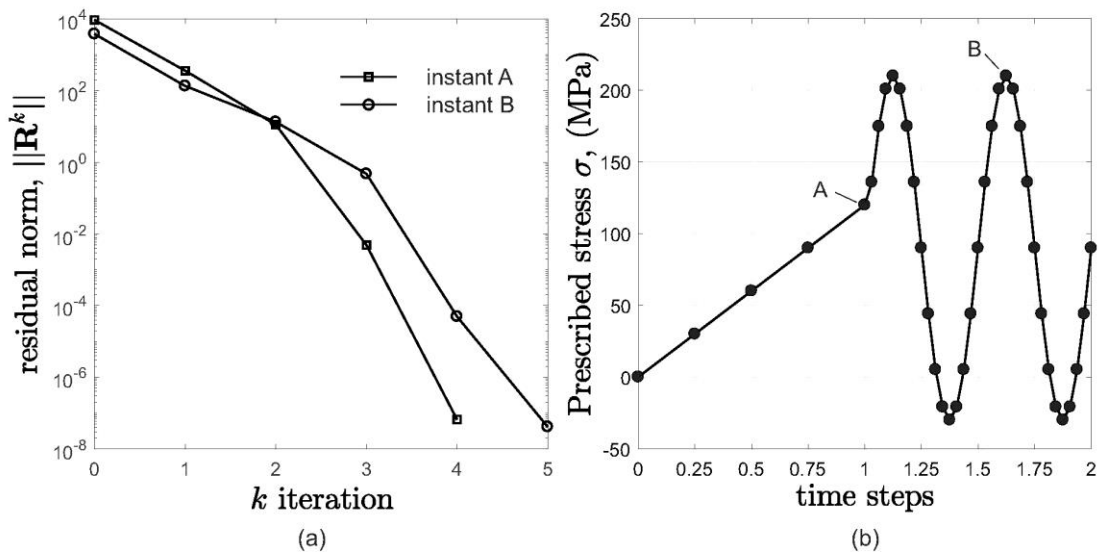


Figure 9. (a) Convergence behaviour of the FE Newton-Raphson scheme for the different instants (b) A and B.

5. Final remarks

This paper presented the formulation and all the necessary tools for the implicit implementation of Chaboche's kinematic hardening model in the context of FE analysis. A detailed strategy for the computation of the consistent tangent operator, which is essential to ensure quadratic rates of convergence of the FE analysis, has been presented. Two very simple examples were assessed in order to validate the numerical implementations. In this case, direct comparisons with analytical solutions allowed the validation of the numerical procedure here described. A third example containing a stress raiser was also investigated in an attempt to evaluate the numerical model capabilities when dealing with more complex problems. In this case, once the material experience high levels of plastic flow near the notch root, residual strains at this region cause a stress relief (Liao *et al.*, 2020), which was properly accounted by the numerical model. It has been also shown that, at least for the studied cases here investigated, integration of the elastoplastic equations by considering a fully implicit or a standard trapezoidal scheme lead to nearly the same results. In this case, the choice of the fully implicit strategy ($\alpha = 1$) seems more advantageous once it produces shorter equations, which in turn implies in fewer calculations.

Appendix A

The Hooke's matrix is given by:

$$\mathbf{D} = \begin{bmatrix} \lambda + 2\mu & \lambda & \lambda & 0 & 0 & 0 \\ 0 & \lambda + 2\mu & \lambda & 0 & 0 & 0 \\ \lambda & \lambda & \lambda + 2\mu & 0 & 0 & 0 \\ 0 & 0 & 0 & \mu & 0 & 0 \\ 0 & 0 & 0 & 0 & \mu & 0 \\ 0 & 0 & 0 & 0 & 0 & \mu \end{bmatrix} \quad (60)$$

where λ and μ are the Lamé constants:

$$\lambda = \frac{E\nu}{(1+\nu)(1-2\nu)}, \quad \mu = \frac{E}{2(1+\nu)} \quad (61)$$

The deviatoric matrix is given by:

$$\mathbf{P} = \frac{1}{3} \begin{bmatrix} 2 & -1 & -1 & 0 & 0 & 0 \\ -1 & 2 & -1 & 0 & 0 & 0 \\ -1 & -1 & 2 & 0 & 0 & 0 \\ 0 & 0 & 0 & 3 & 0 & 0 \\ 0 & 0 & 0 & 0 & 3 & 0 \\ 0 & 0 & 0 & 0 & 0 & 3 \end{bmatrix} \quad (62)$$

The transformation \mathbf{Q} is given by:

$$\mathbf{Q} = \begin{bmatrix} 1 & 0 & 0 & 0 & 0 & 0 \\ 0 & 1 & 0 & 0 & 0 & 0 \\ 0 & 0 & 1 & 0 & 0 & 0 \\ 0 & 0 & 0 & 2 & 0 & 0 \\ 0 & 0 & 0 & 0 & 2 & 0 \\ 0 & 0 & 0 & 0 & 0 & 2 \end{bmatrix} \quad (63)$$

The derivative of the residuals are:

$$\frac{\partial \mathbf{R}_{\sigma_{n+1}}}{\partial \sigma_{n+1}} = \mathbf{I} + \alpha \Delta \gamma \mathbf{D} \frac{\partial \mathbf{N}_{n+1}}{\partial \sigma_{n+1}} \quad (64)$$

$$\frac{\partial \mathbf{R}_{\sigma_{n+1}}}{\partial \boldsymbol{\beta}_{j,n+1}} = \alpha \Delta \gamma \mathbf{D} \frac{\partial \mathbf{N}_{n+1}}{\partial \boldsymbol{\beta}_{j,n+1}} \quad (65)$$

$$\frac{\partial \mathbf{R}_{\sigma_{n+1}}}{\partial \Delta \gamma} = \mathbf{D} [\alpha \mathbf{N}_{n+1} + (1 - \alpha) \mathbf{N}_n] \quad (66)$$

$$\frac{\partial \mathbf{R}_{\beta_{i,n+1}}}{\partial \sigma_{n+1}} = -\frac{2}{3} H_i \alpha \Delta \gamma \mathbf{Q}^{-1} \frac{\partial \mathbf{N}_{n+1}}{\partial \sigma_{n+1}} \quad (67)$$

$$\frac{\partial \mathbf{R}_{\beta_{i,n+1}}}{\partial \boldsymbol{\beta}_{j,n+1}} = \delta_{ij} \left(1 + \sqrt{\frac{2}{3}} b_i \alpha \Delta \gamma \right) \mathbf{I} - \frac{2}{3} H_i \alpha \Delta \gamma \mathbf{Q}^{-1} \frac{\partial \mathbf{N}_{n+1}}{\partial \boldsymbol{\beta}_{j,n+1}} \quad (68)$$

$$\frac{\partial \mathbf{R}_{\beta_{i,n+1}}}{\partial \Delta \gamma} = -\frac{2}{3} H_i \mathbf{Q}^{-1} [\alpha \mathbf{N}_{n+1} + (1 - \alpha) \mathbf{N}_n] + \sqrt{\frac{2}{3}} b_i [\alpha \boldsymbol{\beta}_{i,n+1} + (1 - \alpha) \boldsymbol{\beta}_{i,n}] \quad (69)$$

$$\frac{\partial R_{f_{n+1}}}{\partial \sigma_{n+1}} = \mathbf{N}_{n+1}^T \quad (70)$$

$$\frac{\partial R_{f_{n+1}}}{\partial \boldsymbol{\beta}_{j,n+1}} = -\mathbf{N}_{n+1}^T \quad (71)$$

$$\frac{\partial R_{f_{n+1}}}{\partial \Delta \gamma} = 0 \quad (72)$$

where

$$\frac{\partial \mathbf{N}_{n+1}}{\partial \boldsymbol{\sigma}_{n+1}} = \frac{\mathbf{Q}}{\sqrt{\boldsymbol{\xi}^T \mathbf{Q} \boldsymbol{\xi}}} \left(\mathbf{P} - \frac{\boldsymbol{\xi} \boldsymbol{\xi}^T}{\boldsymbol{\xi}^T \mathbf{Q} \boldsymbol{\xi}} \mathbf{Q} \right) \quad (73)$$

$$\frac{\partial \mathbf{N}_{n+1}}{\partial \boldsymbol{\beta}_{j,n+1}} = \frac{\mathbf{Q}}{\sqrt{\boldsymbol{\xi}^T \mathbf{Q} \boldsymbol{\xi}}} \left(\frac{\boldsymbol{\xi} \boldsymbol{\xi}^T}{\boldsymbol{\xi}^T \mathbf{Q} \boldsymbol{\xi}} \mathbf{Q} - \mathbf{I} \right) \quad (74)$$

$$\boldsymbol{\xi} = \mathbf{S}_{n+1} - \boldsymbol{\beta}_{n+1} \quad (75)$$

and δ_{ij} in Eq. (68) is the Kronecker delta.

Appendix B

For plane stress assumptions, let one defines the following relevant matrices:

$$\boldsymbol{\sigma} = [\sigma_x \quad \sigma_y \quad \tau_{xy}]^T \quad (76)$$

$$\boldsymbol{\beta}_i = [\beta_{i,x} \quad \beta_{i,y} \quad \beta_{i,xy}]^T \quad (77)$$

$$\boldsymbol{\varepsilon} = [\varepsilon_x \quad \varepsilon_y \quad 2\varepsilon_{xy}]^T \quad (78)$$

$$\boldsymbol{\varepsilon}^p = [\varepsilon_x^p \quad \varepsilon_y^p \quad 2\varepsilon_{xy}^p]^T \quad (79)$$

$$\mathbf{S} = \mathbf{P} \boldsymbol{\sigma} \quad (80)$$

where

$$\mathbf{P} = \frac{1}{3} \begin{bmatrix} 2 & -1 & 0 \\ -1 & 2 & 0 \\ 0 & 0 & 3 \end{bmatrix} \quad (81)$$

Through the definition of the following matrix:

$$\mathbf{L} = \begin{bmatrix} 2 & 1 & 0 \\ 1 & 2 & 0 \\ 0 & 0 & 2 \end{bmatrix} \quad (82)$$

the yield function can be expressed as:

$$f = \sqrt{(\mathbf{S} - \boldsymbol{\beta})^T \mathbf{L} (\mathbf{S} - \boldsymbol{\beta})} - \sqrt{\frac{2}{3}} \bar{\sigma}_y \quad (83)$$

From the associative hardening rule:

$$\mathbf{N} = \frac{\mathbf{Q} (\mathbf{S} - \boldsymbol{\beta})}{\sqrt{(\mathbf{S} - \boldsymbol{\beta})^T \mathbf{L} (\mathbf{S} - \boldsymbol{\beta})}} \quad (84)$$

where

$$\mathbf{Q} = \begin{bmatrix} 1 & 0 & 0 \\ 0 & 1 & 0 \\ 0 & 0 & 2 \end{bmatrix} \quad (85)$$

Notice as well that Hooke's matrix under plane stress conditions is given by:

$$\mathbf{D} = \frac{E}{1 - \nu^2} \begin{bmatrix} 1 & \nu & 0 \\ \nu & 1 & 0 \\ 0 & 0 & \frac{1 - \nu}{2} \end{bmatrix} \quad (86)$$

For the resolution of the elastoplastic problem when considering plane stress constraints, one needs to solve a nonlinear system very similar to the one formed by Eqs. (19)-(21). However, in this case, \mathbf{Q} and \mathbf{D} are given by Eqs. (85) and (86), respectively, as well as the residual of the yield function must be replaced by:

$$R_{f_{n+1}} = \sqrt{(\mathbf{S}_{n+1} - \boldsymbol{\beta}_{n+1})^T \mathbf{L} (\mathbf{S}_{n+1} - \boldsymbol{\beta}_{n+1})} - \sqrt{\frac{2}{3}} \bar{\sigma}_y \quad (87)$$

The solution procedure for the nonlinear system formed by the residuals with unknowns $\boldsymbol{\sigma}_{n+1}$, $\boldsymbol{\beta}_{n+1}$ and $\Delta\gamma$ is presented in Subsection 2.2. The derivatives of the residuals are given by expressions Eq.(64)-(72) except by $\partial R_f / \partial \boldsymbol{\beta}_j$ in Eq. (71) that must be replaced by:

$$\frac{\partial R_{f_{n+1}}}{\partial \boldsymbol{\beta}_{j,n+1}} = - \frac{\boldsymbol{\xi}^T \mathbf{L}}{\sqrt{\boldsymbol{\xi}^T \mathbf{L} \boldsymbol{\xi}}} \quad (88)$$

where $\boldsymbol{\xi}$ is given by Eq. (75). In addition, expressions for $\partial \mathbf{N}_{n+1} / \partial \boldsymbol{\sigma}_{n+1}$ (Eq. (73)) and $\partial \mathbf{N}_{n+1} / \partial \boldsymbol{\beta}_{j,n+1}$ for plane stress conditions becomes:

$$\frac{\partial \mathbf{N}_{n+1}}{\partial \boldsymbol{\sigma}_{n+1}} = \frac{\mathbf{Q}}{\sqrt{\boldsymbol{\xi}^T \mathbf{L} \boldsymbol{\xi}}} \left(\mathbf{P} - \frac{\boldsymbol{\xi} \boldsymbol{\xi}^T}{\boldsymbol{\xi}^T \mathbf{L} \boldsymbol{\xi}} \mathbf{Q} \right) \quad (89)$$

$$\frac{\partial \mathbf{N}_{n+1}}{\partial \boldsymbol{\beta}_{j,n+1}} = \frac{\mathbf{Q}}{\sqrt{\boldsymbol{\xi}^T \mathbf{L} \boldsymbol{\xi}}} \left(\frac{\boldsymbol{\xi} \boldsymbol{\xi}^T}{\boldsymbol{\xi}^T \mathbf{L} \boldsymbol{\xi}} \mathbf{L} - \mathbf{I} \right) \quad (90)$$

It is worth noting that, for the computation of the consistent tangent matrix (Subsection 2.3) under plane stress assumptions, \mathbf{M}_{32} in Eq. (45) must be replaced by:

$$\mathbf{M}_{32} = \frac{\partial f}{\partial \boldsymbol{\beta}_j}, \quad \frac{\partial f}{\partial \boldsymbol{\beta}_j} = - \frac{\boldsymbol{\xi}^T \mathbf{L}}{\sqrt{\boldsymbol{\xi}^T \mathbf{L} \boldsymbol{\xi}}} \quad (91)$$

Appendix C

For the uniaxial tension/compression case, Chaboche's kinematic hardening rule terms in the loading direction can be expressed as:

$$\dot{\beta}_i = H_i \dot{\varepsilon}^p \mp b_i \beta_i \dot{\varepsilon}^p \quad (92)$$

where the $-$ sign stands for positive values of $\dot{\varepsilon}^p$ and the $+$ one otherwise. Note that Eq. (92) is a non-exact ordinary differential equation, which can be reduced to its exact form and solved analytically. In this setting, the following expression for the back stress terms can be obtained:

$$\beta_i = \pm \frac{H_i}{b_i} + \left(\beta_{i,0} \mp \frac{H_i}{b_i} \right) \exp[\mp (\varepsilon^p - \varepsilon_0^p)] \quad (93)$$

where the first choice of signals holds for $(\varepsilon^p - \varepsilon_0^p)$ positive and the second one stands for negative values of $(\varepsilon^p - \varepsilon_0^p)$. $\beta_{i,0}$ and ε_0^p come from the initial value problem. In addition, from the yield criterion one has that:

$$\left| \sigma - \sum_{i=1}^m \beta_i \right| = \bar{\sigma}_y \quad (94)$$

Therefore, a closed form expression for σ is given by:

$$\sigma = \sum_{i=1}^m \left\{ \pm \frac{H_i}{b_i} + \left(\beta_{i,0} \mp \frac{H_i}{b_i} \right) \exp[\mp (\varepsilon^p - \varepsilon_0^p)] \right\} \pm \bar{\sigma}_y \quad (95)$$

In general, the use of two nonlinear terms and one linear term in the construction of the kinematic hardening rule is already enough to properly characterize the material behaviour (Chaboche, 1986). In this case, Eq. (95) becomes:

$$\sigma = \sum_{i=1}^2 \left\{ \pm \frac{H_i}{b_i} + \left(\beta_{i,0} \mp \frac{H_i}{b_i} \right) \exp[\mp b_i (\varepsilon^p - \varepsilon_0^p)] \right\} + H_3 (\varepsilon^p - \varepsilon_0^p) \pm \bar{\sigma}_y \quad (96)$$

For pure shear conditions, following the previous steps leads to a similar expression for the shear stress τ . However, notice that in this case, H_i terms in the above equations must be replaced by $2/3 H_i$, b_i by $2/\sqrt{3} b_i$ and $\bar{\sigma}_y$ by $\bar{\tau}_y = \bar{\sigma}_y / \sqrt{3}$.

Appendix D

Particularizing Eq. (96) for a stabilized cycle under fully reversed loading conditions, we find the following expression:

$$\sigma_a = \frac{H_1}{b_1} \tanh(b_1 \varepsilon_a^p) + \frac{H_2}{b_2} \tanh(b_2 \varepsilon_a^p) + H_3 \varepsilon_a^p + \bar{\sigma}_y, \quad (97)$$

where σ_a and ε_a^p are the stress and plastic strain amplitudes, respectively. Therefore, experimental data containing σ_a vs. ε_a^p points can be used to fit Eq. (97) allowing the determination of parameters H_i , b_i and $\bar{\sigma}_y$.

In Section 4, for the resolution of the numerical examples, σ_a vs. ε_a^p experimental data from (Jiang and Zhang, 2008) for an Al7075-T651 alloy have been used to calibrate parameters of Eq. (97). Figure 10 depicts such data fitted by Ramberg-Osgood curve. The smother Ramberg-Osgood curve could then be used to fit Eq. (97) resulting in $H_{1-3} = 8.10(10^3), 66.7(10^3), 160(10^3)$ (MPa), $b_{1-3} = 129.8, 939.7$ and $\bar{\sigma}_y = 431$ (MPa).

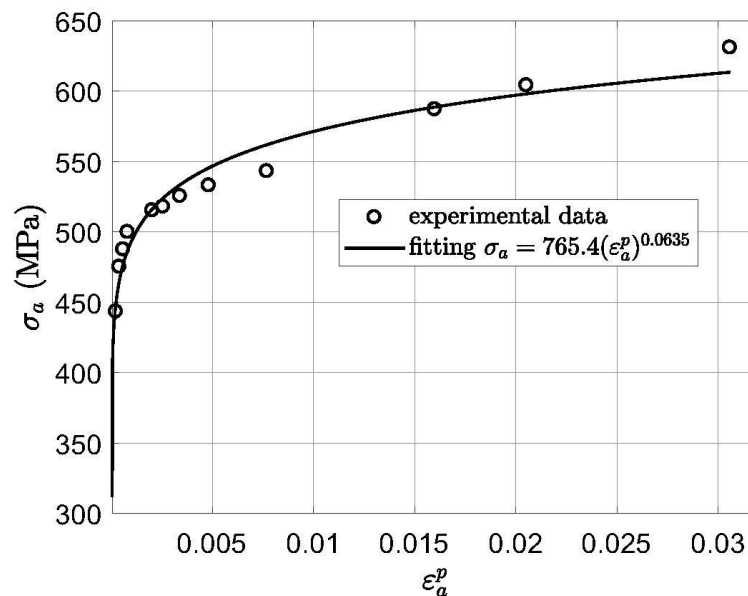


Figure 10. Stabilized stress-strain amplitude data for the AL7075-T651 (Jiang and Zhang, 2008).

References

1. Prager, W. Recent developments in the mathematical theory of plasticity. *J Appl Phys* 1949, 20, 235-241. (<https://doi.org/10.1063/1.1698348>)
2. Armstrong, P.J.; Frederick, C. A mathematical representation of the multiaxial Bauschinger effect. GEGB report RD/B/N731 1966.
3. Chaboche, J. L. Time-independent constitutive theories for cyclic plasticity. *Int J of Plasticity* 1986, 2, 149-188. ([https://doi.org/10.1016/0749-6419\(86\)90010-0](https://doi.org/10.1016/0749-6419(86)90010-0))
4. Wilkins, M.L. Calculation of elastic-plastic flow. Tech Rep University of California, 1963.
5. Simo, J.; Taylor, R. A return-mapping algorithm for plane stress elastoplasticity. *Int J Numer Meth Eng* 1986, 22, 649-670. (<https://doi.org/10.1002/nme.1620220310>)
6. Malcher, L.; Mamiya, E. An improved damage evolution law based on continuum damage mechanics and its dependence on both stress triaxiality and the third invariant. *Int J of Plasticity* 2014, 56, 232-261. (<https://doi.org/10.1016/j.jiplas.2014.01.002>)
7. Lopes, J.; Malcher, L. Fatigue life estimates under non-proportional loading through continuum damage evolution law. *Theor Appl Fract Mec* 2017, 88, 64-73. (<https://doi.org/10.1016/j.tafmec.2016.12.003>)
8. Souza Neto, E. A.; Peric, D.; Owen, D.R. Computational methods for plasticity: theory and applications. John Wiley & Sons, 2011.
9. Hartmann, S.; Haupt, P. Stress computation and consistent tangent operator using non-linear kinematic hardening models. *Int J Numer Meth Eng* 1993, 36, 3801-3814. (<https://doi.org/10.1002/nme.1620362204>)
10. Hopperstad, O. S.; Remseth, S. A return mapping algorithm for a class of cyclic plasticity models. *Int J Numer Meth Eng* 1995, 38, 549-564. (<https://doi.org/10.1002/nme.1620380404>)

11. Ohno, N.; Tsuda, M.; Kamei, T. Elastoplastic implicit integration algorithm applicable to both plane stress and three-dimensional stress states. *Finite Elem Anal Des* 2013, 66, 1-11. (<https://doi.org/10.1016/j.finel.2012.11.001>)
12. Doghri, I. Fully implicit integration and consistent tangent modulus in elasto-plasticity. *Int J Numer Meth Eng* 1993, 36, 3915-3932. (<https://doi.org/10.1002/nme.1620362210>)
13. Fish, J.; Belytschko, T. *A first course in finite elements*. Wiley, 2007.
14. Kim, N.H. *Introduction to nonlinear finite element analysis*. Springer Science & Business Media, 2014.
15. Jiang, Y.; Zhang, J. Benchmark experiments and characteristic cyclic plasticity deformation. *Int J of Plasticity* 2008, 24, 1481-1515. (<https://doi.org/10.1016/j.ijplas.2007.10.003>)
16. Liao, D.; Zhu, S. P.; Correia, J. A.; De Jesus, A. M.; Berto, F. Recent advances on notch effects in metal fatigue: A review. *Fatigue Fract Eng M* 2020, 43, 637-659. (<https://doi.org/10.1111/ffe.13195>)